Mon. Not. R. Astron. Soc. **000**, 000–000 (1997) Printed 1 February 2008 (MN LATEX style file v1.4)

New diagnostic methods for emission-line galaxies in deep surveys

Cláudia S. Rola[1,2], Elena Terlevich[1] & Roberto J. Terlevich[2]

[1] *Institute of Astronomy, University of Cambridge, Madingley Road, Cambridge CB3 0HA, United Kingdom (crola or et @ast.cam.ac.uk)*

[2] *Royal Greenwich Observatory, Madingley Road, Cambridge CB3 0EZ, United Kingdom (rjt@ast.cam.ac.uk)*

Accepted March 1997, Received November 1996

ABSTRACT

We present new quantitative classification methods for emission-line galaxies, which are specially designed to be used in deep galaxy redshift surveys. A good segregation between starbursts and active galactic nuclei, i.e. Seyferts 2 and LINERs, is obtained from diagnostic diagrams involving the [O II]λ3727 $\AA$, [Ne III]λ3869 $\AA$, Hβ and [O III]λ5007 $\AA$ relative intensities or the [O II]λ3727 $\AA$ and Hβ equivalent widths. Furthermore, the colour index of the continuum underlying [O II]λ3727 $\AA$ and Hβ provides an additional separation parameter between the two types of emission-line galaxies.

We have applied the equivalent widths method to the $0 < z \leq 0.3$ emission-line galaxies of the Canada-France Redshift Survey. Our results are in very good agreement with those obtained using the standard diagnostic diagrams including all the strong optical emission-line intensity ratios.

Key words: surveys – H II regions – galaxies: active – galaxies: starburst – galaxies: Seyfert

1 INTRODUCTION

Deep redshift surveys have produced in the past few years a relatively large number of optical/near UV spectra of galaxies at redshifts $z < 0.7 - 0.8$ (e.g., Dressler & Gunn 1983; Couch & Sharples 1987; Broadhurst, Ellis & Shanks 1988; Lavery & Henry 1988; Colless et al. 1990; Colless *et al.* 1993; Songaila *et al.* 1994; Glazebrook *et al.* 1995; Le Fèvre *et al.* 1995). A large percentage of galaxies in these deep surveys present narrow emission lines. The analysis of the spectrum of these distant emission-line galaxies (hereafter ELGs) should provide important information about their intrinsic properties (stellar population, rate of star formation, metallicity, etc.) and the evolution of these parameters with increasing look-back time. But a central problem is that very little is known about the nature, either H II galaxies or active galaxies*, of the ELGs discovered in these deep surveys.

In H II galaxies the emission-line spectrum is dominated by the emission originating in H II regions, where ultraviolet photons emitted by OB stars ionise the surrounding gas, while in the case of active galaxies the gas ionising source is much harder and has the shape of a power law. Furthermore, star forming regions are always associated with H II regions and notably with H II galaxies, while that is not necessarily the case for active galaxies. By determining the different nature (active or H II galaxy) of the ELGs observed in redshift surveys, one can obtain a more precise physical picture of the galaxy evolution process.

Nearby ELGs are classified using the emission-line ratios of the most prominent optical lines like: [O I]λ6300 $\AA$, [O II]$\lambda\lambda$3727, 3729 $\AA$, [O III]$\lambda\lambda$4959, 5007 $\AA$, [N II]λ6584 $\AA$, [S II]$\lambda\lambda$6717, 6730 $\AA$, Hα and Hβ (see Baldwin, Philips & Terlevich 1985; Veilleux & Osterbrock 1987). In higher redshift objects, however, most of these lines move out of the readily observable optical spectral range making impossible the use of current methods to classify ELGs beyond $z \approx 0.3$. For $z > 0.3$ the only strong emission-lines remaining in the optical range are Hβ and [O III]$\lambda\lambda$4959, 5007 $\AA$, observable up to $z \approx 0.7$, and [O II]$\lambda\lambda$3727, 3729 $\AA$ and [Ne III]λ3869 $\AA$ observable up to $z \approx 1.2$. Typical deep redshift survey spec-

* In this paper, we will call active galaxies those hosting an active galactic nucleus (AGN). These are Seyferts 2 and LINERs – Low Ionisation Narrow Emission-line Regions – and we excluded Seyferts 1 as these are generally easier to identify because they present broader Balmer lines (FWHM $> 1,000$ Km s^{-1}).

tra have a low signal-to-noise ratio, so they usually show only the two strongest emission lines, like [O II]λ3727 $\AA$ † and Hβ, rendering the existent methods of classification useless. Nevertheless, in spite of not being able to determine their nature, the large values of EW([O II]) observed in ELGs at intermediate redshifts lead researchers to suggest high rates of present star formation and therefore the existence of a significant fraction of starburst galaxies (e.g., Broadhurst *et al.* 1988, Colless *et al.* 1990).

However, it is important to remember that the intensity or the equivalent width of an emission-line is related to the present star formation rate *only* if the ionisation *and* observed continuum sources are OB stars as is the case in H II galaxies (i. e., starburst galaxies, blue compact galaxies, etc), which is not necessarily the case for galaxies hosting an AGN (i.e. Seyferts type 1 and 2, and LINERs).

Tresse *et al.* (1996) analysed the Canada-France Redshift Survey (CFRS) galaxies up to a redshift of 0.3 and found that about 17 % of all objects have emission-line ratios consistent with being active galaxies (like Seyferts 2 or LINERs). Unlike in previous deep redshift surveys, a classification was possible thanks to the wide spectral range observed (4500 - 8500 $\AA$) which allowed to use the classical diagnostic diagrams (see also Rola, 1995). Their result indicates that in deep surveys the fraction of ELGs that are active galaxies may be higher than previously thought. It becomes therefore very important to compare the CFRS results with other surveys and to extend this analysis to higher redshifts. To accomplish this it is necessary first to find new diagnostic methods that are appropriate for deep surveys and could properly separate active galaxies from H II galaxies at $z > 0.3$.

In this paper we investigate new methods of quantitative classification that involve only the strong emission-lines that can be detected in deep redshift surveys, as well as the continuum colour. As reference we used a large sample of nearby ELGs, comprising 231 high quality spectra of H II galaxies, Seyfert 2 nuclei and LINERs, classified combining the usual diagnostic diagrams method with an extended grid of photoionisation models. Section 2 explains the methodology used. Section 3 describes the characteristics of the sample of ELGs used in our study and explains how the classification of the reference local sample of ELGs was made. Section 4 presents the new diagnostic diagrams and discusses the advantages and the problems of the new methods. Conclusions are drawn in section 5.

2 METHODOLOGY

The main steps in the methodology used in this work are the following. We have first compiled a quality sample of local emission-line spectra in which we performed a reliable classification of the nature of the ELGs. This classification is based on a purpose built grid of photoionization models, allowing an improved approach compared with the usual empirical methods.

After classifying the nearby sample into 3 groups of objects: definite H II galaxies, definite active galaxies (Seyferts 2 and LINERs) and intermediate objects, we analysed the definite H II galaxies and active galaxies sets, in order to search for new diagnostics to identify the nature of ELG's involving **only** lines to the blue of 5000 $\AA$, approximately. This is because we want the new diagnostic methods to be applicable to optical redshift surveys up to $z \approx 0.75$. In order for the new methods to be also applicable to spectra which are not flux calibrated we have built some diagnostic methods based only on the equivalent widths of certain emission-lines. For the flux calibrated data, the new methods use also emission-line intensity ratios and/or the continuum intensity.

While building this compilation of emission-line spectra we have examined all the published data on H II galaxies and active galaxies. As we are interested in the nature segregation, we used only the best available optical data in terms of emission-line spectra. Therefore, we opted to use spectra with good data in the region 3600 $\AA$ to 5100 $\AA$. Nevertheless, this is not often easy to obtain. To begin with, until very recently only a few detectors/spectrographs had high sensitivity in the region from 3600 $\AA$ to 4000 $\AA$. On top of that, most observers do not publish the equivalent widths of the strongest lines, so the information about the continuum shape is lost.

3 REFERENCE SAMPLE: CHARACTERISTICS AND NATURE CLASSIFICATION

The data sample we used in this work comes mainly from the Terlevich *et al.* (1991) spectrophotometric catalogue of H II galaxies (where some AGNs are also included), selected using slitless spectroscopy. Additional ELGs come from the Cambridge survey (see Masegosa *et al.* 1994). The data for typical AGN's was augmented using published spectrophotometry from Ho *et al.* (1993) and Costero & Osterbrock (1977). The condition (trivial) imposed for an object to be included in the final sample was that the data had to contain the lines to be used in the new methods, i. e., at least [O II]λ3727 $\AA$, [Ne III]λ3869 $\AA$, Hβ and [O III]λ5007 $\AA$ and the equivalent widths of [O II]λ3727 $\AA$ and Hβ. One large problem found is that there is in the literature only a handful of AGNs with measurements of the equivalent widths of [O II]λ3727 $\AA$ and Hβ.

For the classification of the sample four diagnostic diagrams were used: [O III]λ5007/Hβ versus [S II]λ6725/Hα‡, [O III]λ5007/Hβ versus [N II]λ6583/Hα, [O III]λ5007/Hβ versus [O I]λ6300/Hα and [O III]λ5007/Hβ versus [O II]λ3727/Hβ§ (see Baldwin, Philips & Terlevich 1985, Veilleux & Osterbrock 1987 and Rola 1995). These are presented in figure 1 with the curves determined from the photoionisation models, separating the H II galaxies region from the active galaxies region (see following section for details).

† Hereafter, [O II]λ3727 $\AA$ represents the sum of the lines [O II]$\lambda\lambda$3727, 3729 $\AA$.

‡ [S II]λ6725 $\AA$ represents the sum of the lines [S II]$\lambda\lambda$6717, 6731 $\AA$

§ intensity ratio corrected for reddening

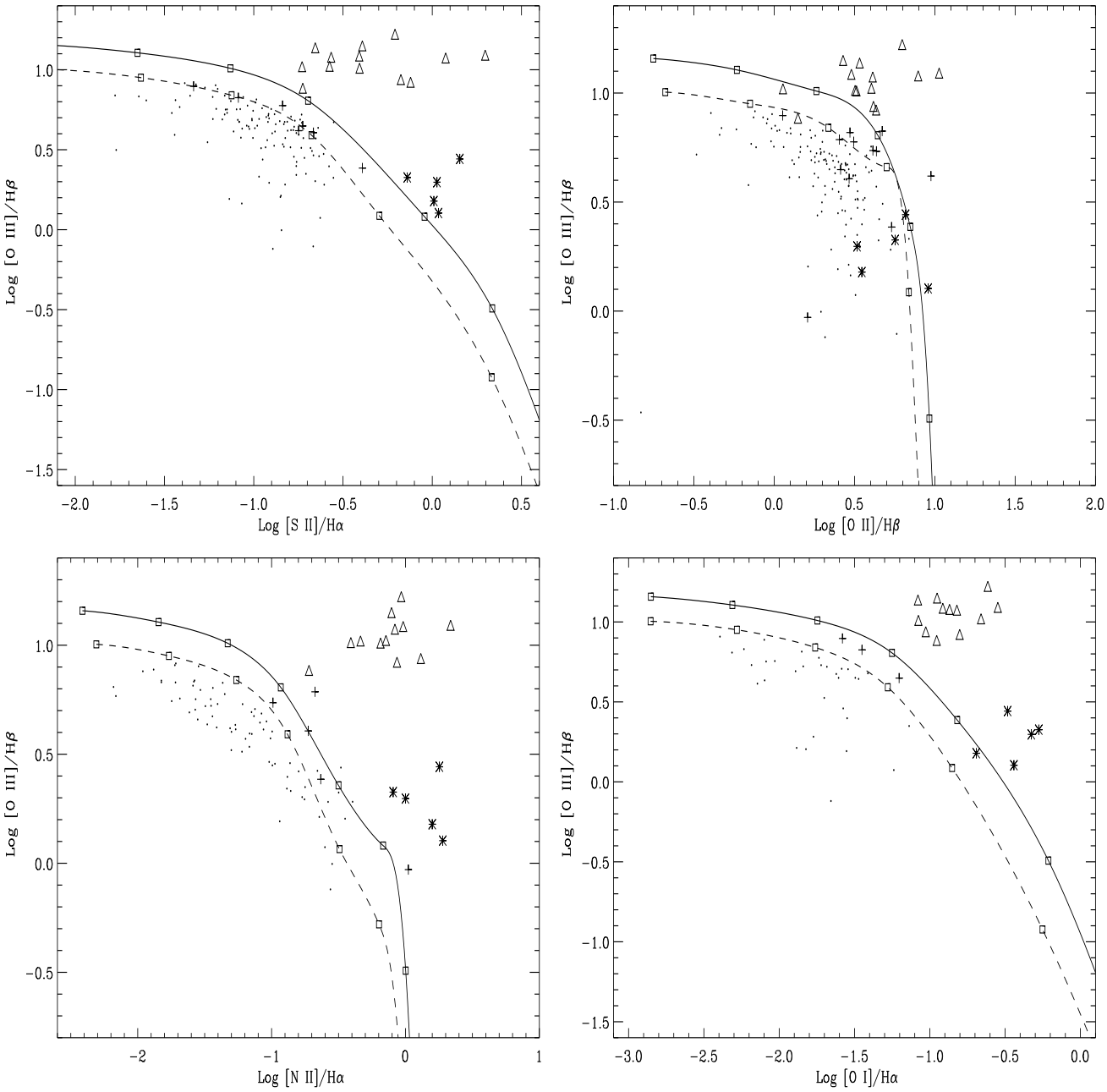

Figure 1. The four diagnostic diagrams used in the classification of the reference sample. The curves correspond to photoionisation by OB stars, for stellar effective temperatures of 50,000 K (dashed line) and 60,000 K (full line) respectively (see text). The ELGs classified as Seyfert 2 are represented by triangles, LINERs by asterisks and the dots are H II galaxies; crosses mark the transition or ambiguously classified objects.

3.1 Photoionisation models

We have determined the boundary between H II galaxies and active galaxies in the diagnostic diagrams using an extensive grid of steady-state spherically symmetric H II region photoionization models computed with the code PHOTO (see Rola 1995 and Stasińska 1990). To mimic the complexity of H II galaxies and best determine their loci in the diagnostic diagrams, we have considered wide ranges for the physical parameters of the models.

There are five main parameters driving the photoionization models used to determine the loci of H II galaxies in the diagnostic diagrams: the hydrogen density (n_H), the metallicity (Z), the number of ionizing stars (N), the filling factor (f) and the ionizing source effective temperature ($T_{\rm eff}$). All the grid models considered a constant hydrogen density, n_H=10 cm^{-3}. Varying n_H in the range found in H II regions (n_H=10 − few 100 cm^{-3}) has a negligible effect on the intensity ratios. Models are dust free (the effects of dust were considered only as depletion) and were calculated using three free parameters, the ionisation parameter, $U = Q_H/(4\pi R^2 n_H c)$ (where Q_H is the number of H^o ionis-

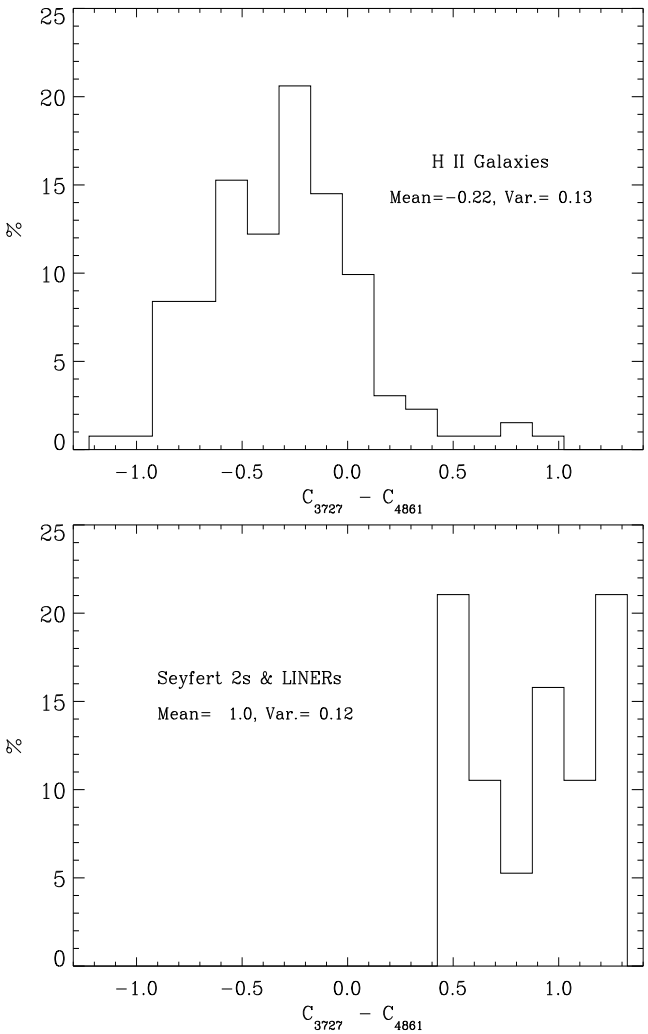

Figure 2. The distribution of the $C_{3727} - C_{4861}$ colour index is shown for H II Galaxies (top) and for active galaxies (bottom). The percentages are relative to the total number of ELGs of each type. The mean and variance of each distribution are shown in the diagrams.

ing photons, R is the radius of the photoionised region and c is the speed of light), the effective temperature of the ionizing radiation, T_{eff}, and the metallicity of the gas, Z. U, which can also be written as $U \propto (n_H f^2 N Q_H^\star)$ (where $Q_H^\star$ is Q_H for a single star and N is the number of ionising stars) varied roughly between 0.2 and 10^{-6}. For simplicity, we have considered the ionising source as a "cluster" with a single type of stellar atmosphere, with T_{eff} ranging from 3×10^4 K to 6×10^4 K. This is a reasonable approximation if the hottest stars are assumed to dominate the total flux of ionising photons. For the distribution of the ionising radiation we have used the $\log g = 5.0$ Kurucz model atmospheres (Kurucz, 1992) with an abundance consistent with the one in the nebula. We considered four metallicities: 2 $Z_\odot$, $Z_\odot$, 0.25 $Z_\odot$ and 0.1 $Z_\odot$. More details about the grid are given in Rola (1995) and in Tresse *et al.* (1996).

3.2 Boundaries between H II galaxies and active galaxies

Uncertainties in the input parameters of the photoionization models such as the stellar atmospheres spectrum and the value of the upper limit for the stellar effective temperature of the hottest stars, as well as in the values of atomic coefficients used in the photoionisation models, mean that the boundary separating H II galaxies from active galaxies cannot be accurately defined. Furthermore, H II galaxies are more complex systems than a H II region with a single type of ionising stellar atmosphere, so these boundaries should be considered with some caution. We have opted for a conservative approach and selected the models that define the limits to the location of H II galaxies in the diagnostic diagrams in a way that slightly overestimates the region occupied by them (therefore, slightly underestimating the active galaxies region).

Two boundary lines were used to segregate the H II galaxies from the active galaxies by their emission-line intensity ratios. They define the "extreme" limits of H II galaxies in the diagnostic diagrams and are obtained from photoionisation models with T_{eff} = 50,000 K or 60,000 K, $Z = 0.25$ and 1 $Z_\odot$, with U varying between 2.0×10^{-6} and 8.0×10^{-2}, approximately¶. The models are shown in figure 1, where the symbols associated with each ELG represent the final classification.

3.3 Sample classification

We have determined the nature of the ELGs in the reference sample considering both T_{eff} = 50,000 K and T_{eff} = 60,000 K boundaries. ELGs in the left part of the diagnostic diagrams are H II galaxies while those in the right are AGNs. Objects which fell between both separation curves in the diagnostic diagrams were considered *transition* objects. This final classification was obtained by considering the balance of the 4 diagrams classification. If an ELG was classified both as an H II and an AGN in an equivalent number of diagrams, its final classification was considered ambiguous, and we called these also *transition* objects. Finally, among AGNs we classified as LINERs those with log [O III]λ5007/H$\beta \leq$ 0.5 (Veilleux & Osterbrock 1987, Filippenko & Terlevich 1993). We remark that our classification criteria for LINERs has been tested and seems equivalent to the original Heckman (1980) criteria, i.e., [O II]λ3727/[O III]λ5007 $\geq$ 1, and [O I]λ6300/[O III]λ5007 $\geq$ 1/3.

Out of the 162 ELGs that meet our selection conditions, we classified 131 as H II galaxies, 14 as Seyferts 2 and 5 as LINERs. 12 objects remained unclassified due to ambiguity in their location in the diagnostic diagrams of Figure 1, i.e., either the classification was not conclusive (they appear as H II galaxies and as AGNs in an equivalent number of diagnostic diagrams) or they were located between the 50, 000 K and the 60, 000 K curves in most of the diagnostic diagrams of figure 1.

¶ Blackbody models with T_{eff} from 100,000 to 150,000 K do not change significantly the location of the H II galaxies upper envelope

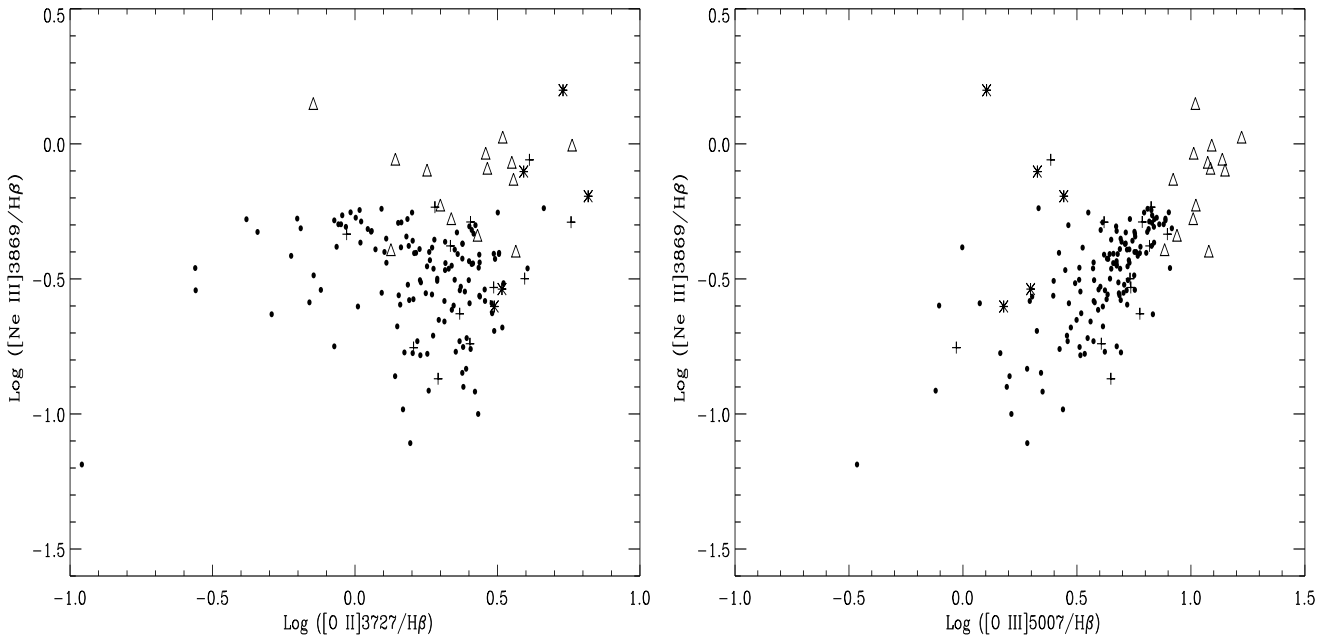

Figure 3. Symbols as in Figure 1. *Left diagram*: [O II]λ3727/Hβ versus [Ne III]λ3869/Hβ intensity ratios. Note that contrary to the top-right diagram of figure 1, the data are not corrected for reddening. There is an upper limit beyond which no more H II galaxies from our sample are observed. This is situated at about log ([Ne III]λ3869/Hβ) ≈ - 0.2. *Right diagram*: [O III]λ5007/Hβ versus [Ne III]λ3869/Hβ intensity ratios (not reddening corrected). The separation limit between H II and active galaxies is the same, but here the [O III]λ5007/Hβ intensity ratio allows to identify LINERs (log ([O III]λ5007/Hβ) ≤ 0.5) from Seyferts 2 (log ([O III]λ5007/Hβ) > 0.5).

4 NEW DIAGNOSTIC DIAGRAMS

For the emission-line reference sample discussed in section 3, a minimum of four emission-line intensities (of which two were Hα and Hβ) were available for the classification of each object. This is usually not the case in most deep redshift surveys. In objects with redshift larger than 0.3, the Hα line falls out of the spectral range of CCD detectors making reliable reddening corrections (as well as object classifications) exceedingly difficult. An other strong emission-line commonly present in ELGs spectra, [O III]λ5007 Å, is lost at z > 0.7, approximately. It is therefore important to be able to determine the nature of redshifted ELGs independently of reddening and using a minimum number of emission-lines between [O II]λ3727 Å and [O III]λ5007 Å. Hence we investigated diagnostic diagrams using the [O II]λ3727 Å, [Ne III]λ3869 Å, Hβ and [O III]λ5007 Å emission-lines and not requiring reddening or stellar absorption corrections. These are the easiest lines to detect in the optical range up to $z \approx 0.75$. We decided to use also equivalent widths (which are essentially reddening independent and do not require flux calibration) instead of using intensity ratios only. In addition we have investigated the use of the colour of the underlying continuum as a classification parameter. *None of the data in any of the new diagrams is reddening or stellar absorption corrected*, so that we would be working in the same conditions with the local sample of ELGs as we would encounter in a redshifted one.

4.1 The blue continuum colour

We have defined the continuum colour index "$C_{3727}-C_{4861}$" as:

$$C_{3727} - C_{4861} = 2.5 \times \log\left(\frac{C_{H\beta}}{C_{[OII]\lambda3727}}\right), \quad (1)$$

where $C_{H\beta}$ is the intensity of the continuum underlying Hβ. Accordingly with the parameters available from our data this was calculated as:

$$C_{3727}-C_{4861} = 2.5\times\log\left(\frac{EW([OII]\lambda3727)}{EW(H\beta)} \times \frac{I_{H\beta}}{I_{[OII]\lambda3727}}\right) (2)$$

where the $\frac{I_{H\beta}}{I_{[OII]\lambda3727}}$ flux calibrated intensity ratio has not been corrected from reddening. With the above definition, larger $C_{3727} - C_{4861}$ values correspond to redder continua.

The distribution of this colour index for our ELGs sample is shown in figure 2, where it can be seen that AGNs tend to have higher values of $C_{3727} - C_{4861}$, i.e. a redder continuum, than H II galaxies. This is potentially an important result for the classification of ELGs; all AGNs in figure 2 have $C_{3727} - C_{4861} \geq 0.4$ against only about 4% of all H II galaxies.

This dichotomy in the colour index distribution is probably a reflection of the fact that in the local Universe while most starburst galaxies have late Hubble types (Sc-Sd), galaxies with AGN tend to be of early Hubble type (Sa-Sc) (Terlevich *et al.* 1987). While red giants contribute significantly to the continuum of the central regions of galaxies with an AGN, young OB stars are the main contributors to the optical continuum of H II galaxies. Accordingly, we suggest that the $C_{3727} - C_{4861}$ colour index provides a valid cri-

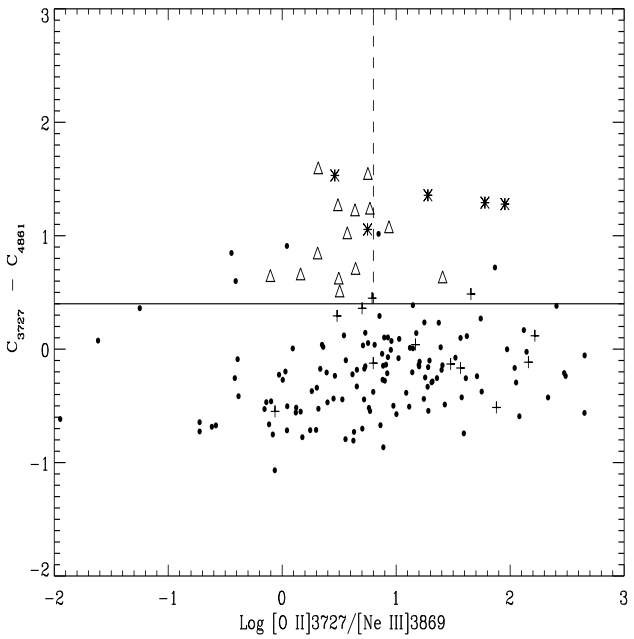

Figure 4. [O II]λ3727/[Ne III]λ3869 intensity ratio versus $C_{3727} - C_{4861}$. Symbols as in Figure 1. The data are not reddening corrected. Reasonably good segregation is attained between LINERs and Seyferts 2 (for log ([O II]λ3727/[Ne III]λ3869) > 0.8 and $C_{3727} - C_{4861} > 0.4$, approximately).

terium to separate AGNs from H II galaxies for local galaxies. However, its behaviour at higher redshift is difficult to predict, specially for the case of AGNs. Therefore, we advise the reader to be cautious when applying this index to redshifted ELGs.

It is possible that similar results may be found by using other continuum colour indices (e.g. Kennicutt 1992). We have used the [O II]λ3727 $\AA$ and Hβ lines because these were the ones for which we maximized the number of ELGs with observed equivalent widths.

4.2 Emission-line ratio diagrams

The strongest emission-lines observed in the near ultraviolet part of the spectrum of ELGs are [O II]λ3727 $\AA$ and [Ne III]λ3869 $\AA$.

The oxygen doublet [O II]λ3727 $\AA$ is particularly intense in objects which contain a large, partially ionised, transition region, like is the case in active galaxies. In this region, high energy photoelectrons, resulting from photoionisation by X-ray photons and by Auger processes, collisionally excite the O^+ ion, along with other atoms/ions like O^0, S^+ and N^+.

The neon [Ne III]λ3869 $\AA$ line is usually more conspicuous in AGNs than in H II galaxies. This may be due to the lack of strong metallic absorption edges in the AGNs ionising continuum compared with the atmospheres of the stars exciting the H II regions where the formation of Ne^{+2} tends to be suppressed relative to O^{+2} (Balick & Snedon, 1976; Shields & Searle, 1978). Additionally, the fact that the ionisation potentials of O^{+2} and Ne^{+2} are relatively close (35.1 eV and 41 eV, respectively) and that [Ne III]λ3869 $\AA$ is also a nebular line, suggests that [O III]λ5007 $\AA$ can be replaced by [Ne III]λ3869 $\AA$ in the diagnostic diagrams of figure 1.

Replacing [O III]λ5007 $\AA$ by the [Ne III]λ3869 $\AA$ line in the [O II]λ3727/Hβ against [O III]λ5007/Hβ diagnostic diagram of figure 1, we obtained a rather similar diagram (although the new diagram is not corrected for reddening and it depends on the Ne/O abundance ratio), which is displayed in figure 3 (left diagram). This new diagram seems also quite efficient in separating active galaxies from H II galaxies. In fact, there is an upper limit situated at log ([Ne III]λ3869/Hβ)$^{\|}$ $\approx$ - 0.2, above which no H II galaxies are observed.

LINERs are quite difficult to separate from Seyferts 2 with so few adequate diagnostic lines as available from deep redshift surveys. Nevertheless, the [O III]λ5007/Hβ intensity ratio (see the right panel of figure 3) allows some level of segregation between LINERs (log ([O III]λ5007/Hβ) $\leq$ 0.5) and Seyferts 2 (log ([O III]λ5007/Hβ) > 0.5). Furthermore, if we now plot the $C_{3727} - C_{4861}$ colour index against the [O II]λ3727/[Ne III]λ3869 line ratio, without correcting them for reddening (see figure 4), we can define three regions in the diagram: one for H II galaxies (the bottom region), one for LINERs (the upper right one) and one for LINERs and Seyferts 2 (the upper left one). We have to be cautious in our conclusions because of the very small sample of LINERs available to us, but it seems that the region limited by log ([O II]λ3727/[Ne III]λ3869) > 0.8 and $C_{3727} - C_{4861} >$ 0.4, approximately, tends to be more populated by LINERs than by the other two types of ELGs.

4.3 Equivalent width diagrams

All the diagrams considered up to now involve the use of emission-line or continuum intensities. Unfortunately, in many of the existent redshift survey data bases the observed spectra are not flux calibrated, which difficults the use of these diagrams. For this reason, we decided to determine other diagnostic diagrams which would overcome this problem by using only equivalent widths.

In figure 5 we plotted EW([O II]λ3727)/EW(Hβ) against EW([O II]) and against EW(Hβ), on the left and right diagrams, respectively. The lines drawn in each diagram define three zones identifying the nature of the ELGs. The horizontal lines were defined according to the distribution of the EW([O II]λ3727)/EW(Hβ) ratio. It is found that about 73 % of all the active galaxies in the sample (against 8% of all H II galaxies) are located above the value of 3.5. The curve and vertical lines in the left and right diagrams, respectively, are based on our data analysis where we have found that an EW(Hβ) of 10 $\AA$ is a good upper limit to separate active galaxies from H II galaxies as only a few H II galaxies lie below this limit. We have tested the validity of this limit, specially to check if our H II galaxies sample is not biased towards the blue, luminous, young H II galaxies ignoring the ones with low EW(Hβ) values. We have concluded that this is not the case, the blue, luminous H II galaxies are randomly distributed in terms of their EW(Hβ) values.

$^{\|}$ intensity ratio not reddening corrected.

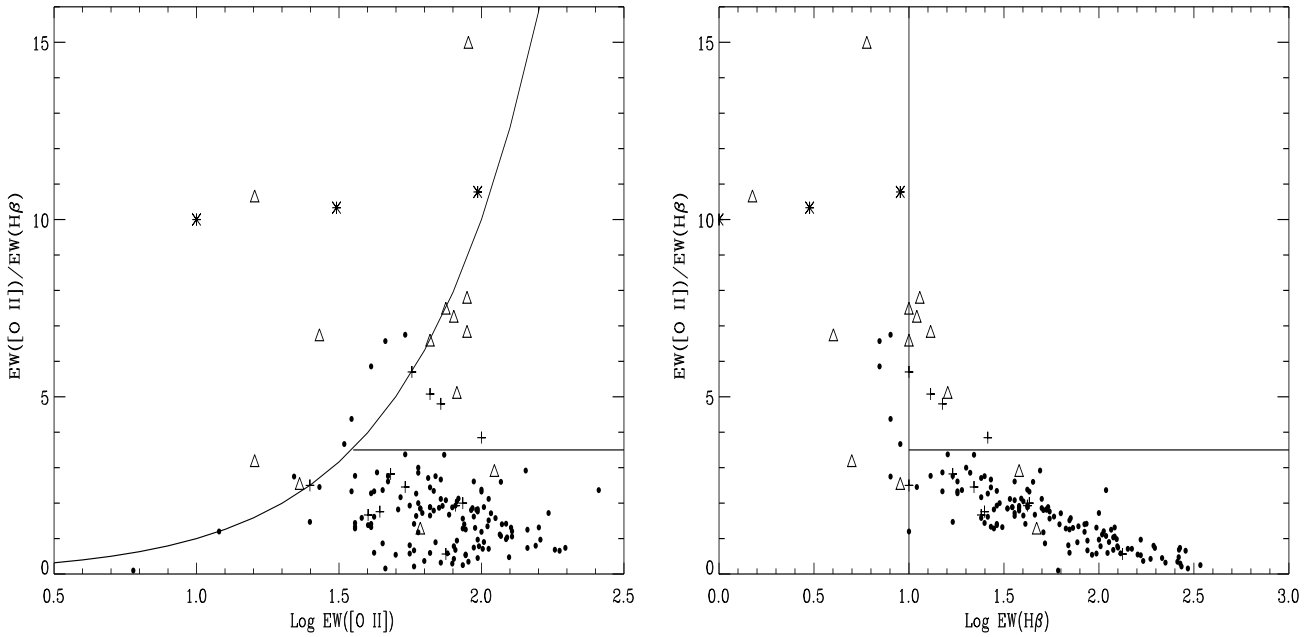

Figure 5. EW([O II]λ3727)/EW(Hβ) ratio versus EW([O II]λ3727 (left diagram) and versus EW(Hβ) (right diagram). In the left diagram, the curve represents the points with EW(Hβ) equal to 10 $\AA$, and objects above it have a lower value. The horizontal line was drawn based on the distribution of the different types of galaxies as a function of the EW([O II]λ3727)/EW(Hβ) ratio, so that most of our active galaxies are located above 3.5. The same separation limits apply to the diagram on the right. Symbols are the same as in Figure 1.

Thus, the combination of the two above mentioned limits leads to the following separation zones in both diagrams of Figure 5. The first one corresponds to the lower right region (henceforth called *H II galaxies region*), where most of the H II galaxies and only a few active ones are located. It is limited upwards by the curve at EW([O II]λ3727)/EW(Hβ) = 3.5 and leftwards by the curve EW(Hβ) = 10 $\AA$. About 87 % of all H II galaxies in our sample are located here against 15 % of all Seyferts 2 and no LINERs (which represent about 12 % of all active galaxies in the data sample).

The second one (hereafter called *AGN region*) corresponds to the sum of two zones. One is defined by the region where EW(Hβ) $\leq$ 10 $\AA$ (left region in diagrams). The other corresponds to the location where EW([O II]λ3727)/EW(Hβ) $\geq$ 3.5 *and* EW(Hβ) $>$ 10 $\AA$ (upper right region in diagrams). About 85 % of all our Seyferts 2 and 100 % of all our LINERs are located here (about 88 % of all our active galaxies) against 13 % of all H II galaxies.

Let us call these percentages "normalised frequencies", as they are calculated as the frequency of ELGs of a certain type, in a certain region, normalised to the total number of ELGs of that type.

Considering that for each *region* the sum of the normalised frequencies, i. e., the normalised frequency of AGNs (Freq$_{\rm region}$(AGN)) *plus* the normalised frequency of H II galaxies (Freq$_{\rm region}$(H II)), is equal to unity, we have made a crude estimate of the "probability" that an ELG which falls in a given *region* of the diagnostic diagram is either an AGN or an H II galaxy. This illustrates the goodness of the diagrams for separating the various types of ELGs. Although from our literature search we believe that our sample is representative of each type of ELG in the local Universe we should keep in mind that these "probabilities" could slightly change if, for example, we add more AGNs to our reference sample. Nevertheless and for the sake of simplicity we will still call these *probabilities*.

This leads to determine that in the AGN region, the probability that an ELG is an AGN is Prob$_{\rm AGN}$(AGN) $\approx$ 87 %, and that of it being an H II galaxy is Prob$_{\rm AGN}$(H II) $\approx$ 13 %, while in the H II galaxies region, Prob$_{\rm H\ II}$(AGN) $\approx$ 12 % and Prob$_{\rm H\ II}$(H II) $\approx$ 88 %.

Most LINERs appear in the left region of the diagrams of Figure 5** i. e., where EW(Hβ) is smaller than 10 and that we call *region AGN I*. Can we use these diagrams to separate LINERs from Seyfert 2 galaxies? In *region AGN I* we find about 11 % of all H II galaxies and about 53 % of all active galaxies, which corresponds to 86 % of all the LINERs and 44 % of all Seyferts 2. In terms of probabilities we have that in *region AGN I*: Prob$_{\rm AGN\ I}$(Seyf. 2) $\approx$ 32 %, Prob$_{\rm AGN\ I}$(LINER) $\approx$ 61 % and Prob$_{\rm AGN\ I}$(H II) $\approx$ 7 %. However, we are dealing with a small number of LINERs which may not be representative of the whole LINERs family.

Region AGN II is the top/right one in the diagrams of Figure 5, limited to those ELGs where EW([O II]λ3727)/EW(Hβ) $\geq$ 3.5 and EW(Hβ) $>$ 10. About 35 % of all active galaxies (corresponding to 41 % of all the Seyfert 2 galaxies and 14 % of all LINERs) and 1 % of all H II galaxies are located here. In terms of probabilities: Prob$_{\rm AGN\ II}$(Seyf. 2) $\approx$ 75 %, Prob$_{\rm AGN\ II}$(LINER) $\approx$ 25 % and Prob$_{\rm AGN\ II}$(H

** Note that some LINERs are located up, out of the visible plotted range in the diagrams.

II) = 0 %. Therefore, this is the region where the probability that an ELG is a Seyfert 2 is maximum.

4.4 Transition/Ambiguous emission-line galaxies

It is important to also consider the behaviour of the 12 transition/ambiguous ELGs of the reference sample (recall subsection 3.3) in the new diagrams. In all of them, from figure 3 to figure 5, these ELGs are located mainly in the H II galaxies region. Although in the equivalent width diagrams of Figure 5 few of the transition/ambiguous objects are placed in the AGN II region, they are all close to the separation limits.

The $C_{3727}-C_{4861}$ colour index distribution of the 12 ambiguous ELGs, range from approximately -0.6 to 0.4 with the mean value 0.01, shows a large superposition with that of the H II galaxies.

Thus, the transition/ambiguous ELGs are located mainly with the H II galaxies in the new diagrams with little spillage over the AGN region. This could lead essentially to three possibilities: 1) these objects are in fact H II/AGN composite, with an AGN component weaker than the emission component produced from ionisation by stellar sources; 2) they are H II galaxies with a peculiar hot stellar population; 3) these galaxies have just different properties in their ionized regions. It is difficult to determine what makes these objects different from H II galaxies; future work will have to address these points.

Nevertheless, a clear conclusion can be drawn: the distribution of the unclassified ELGs strengthens the validity of our new methods for redshift surveys, in the sense that the possibility of finding a transition/ambiguous object in the AGN region of the diagrams is almost negligible.

4.5 Evolutionary effects and application to CFRS sample

Galaxy evolution with redshift may possibly modify the stellar population and gas structure and composition of ELGs, affecting somehow the $C_{3727} - C_{4861}$ colour index, but will not strongly affect emission-line intensity ratios as they depend only on the nebular emission.

It is difficult to predict both how the continuum will evolve and how evolution will affect the equivalent widths of the [O II]λ3727 $\AA$ and Hβ lines. In fact, theoretical models trying to represent evolving H II galaxies do not generally consider important details as the stellar absorption under Hβ, while for Seyferts 2 and LINERs the mechanisms responsible for the gas ionisation are not well known. Nevertheless, it is important to determine the effect of evolution in the continuum and in the equivalent width of these emission-lines in order to understand the physics of the ELGs observed in intermediate and high redshift surveys. This will have to be studied in detail in future work.

In the mean time, we can take an empirical approach and compare the values of the equivalent widths of the [O II]λ3727 $\AA$ and Hβ lines in our sample with the ones obtained in deep redshift surveys (e.g., LDSS: Colless *et al.* 1990 or CFRS: Tresse *et al.* 1996). We notice (see figure 6 below) an absence of survey objects with EW(Hβ) larger than $\approx$ 55 $\AA$ while in the local sample of H II galaxies, the EW(Hβ) reaches values up to $\approx$ 320 $\AA$. This could be a real effect, evidence for galaxy evolution with redshift, or an artifact due to observational selection effects attributed to either instrumentation or most probably to the way samples were selected. At this stage it is impossible to answer these questions. Nevertheless, this is an important issue which deserves future investigation.

In order to test whether the results obtained with the new diagrams of figure 5 are consistent with the ones determined from the standard diagnostic methods, we used the former to classify the CFRS ELGs analysed by Tresse *et al.* 1996 (i.e. those with $z \leq 0.3$). We have plotted in figure 6 the corresponding sub-sample of CFRS ELGs, for which [O II]λ3727 $\AA$ and Hβ have been observed, and their equivalent widths have been measured. Tresse *et al.* (1996) have used standard diagnostic diagrams to separate the AGN from the H II ELGs in their sample. Using our figure 5 diagrams we have found that about 33 % of the galaxies up to $z = 0.3$ are active galaxies. Due to the large abscissa error bars,†† 7 objects are compatible both with being an AGN and an H II galaxy. Excluding them, the fraction of AGNs falls down to about 20 %, which is in quite good agreement with the (mean) 17 % fraction obtained by Tresse *et al.* (1996) using the classical diagnostic diagrams based only on emission-line intensity ratios. Furthermore, if we compare our classification for each CFRS z $\leq$ 0.3 ELG with the one of Tresse *et al.* (1996), we check that these disagree only for 4 objects.

Unfortunately, due to the large error bars in the Tresse *et al.* (1996) sample, it is not possible to draw any conclusions regarding the $C_{3727} - C_{4861}$ colour index.

5 DISCUSSION AND CONCLUSION

The main goal of this work was to investigate new diagnostic methods appropriate to classify the ELGs observed in deep redshift surveys. Most of the more prominent optical lines used in the standard diagnostic diagrams (Baldwin, Philips & Terlevich 1985; Veilleux & Osterbrock 1987) move out of the observable optical spectral range for objects with $z > 0.3$. In fact, for $z > 0.3$ the only strong emission-lines remaining in the optical range are Hβ and [O III]$\lambda\lambda$4959, 5007 $\AA$, observable up to $z \approx$0.7, and [O II]λ3727 $\AA$ and [Ne III]λ3869 $\AA$ observable up to $z \approx$1.2. This implies that the methods used to classify the ELGs observed in redshift surveys will have to be independent of reddening and to rely on a minimum of information from the optical/near ultraviolet part of the spectrum. Hence, we based our study mainly on the [O II]λ3727 $\AA$, [Ne III]λ3869 $\AA$, Hβ and [O III]λ5007 $\AA$ emission-lines and on a new continuum colour index. All of these can be observed with CCD detectors up to a redshift of $\sim$ 0.75.

Using as a reference set a large number of nearby ELGs, we have found that:

a) The $C_{3727} - C_{4861}$ colour index provides a good discriminator between local H II galaxies and active galaxies, i.e. Seyferts 2 and LINERs, while the [O II]λ3727 $\AA$ to [Ne III]λ3869 $\AA$ line intensity ratio segregates between Seyferts

†† For the sake of clarity, we did not plot the abscissa error bars in figure 6.

2 and LINERs. Nevertheless, $C_{3727} - C_{4861}$ should be used with caution for higher redshift galaxies as its behaviour with redshift is difficult to predict, specially for the case of active galaxies.

b) Diagrams using the [Ne III]λ3869/Hβ, [O II]λ3727/Hβ and [O III]λ5007/Hβ intensity ratios provide also reliable classification for ELGs. These have the advantage of depending only on the nebular emission.

c) Good discrimination between AGNs and H II galaxies is provided by the EW([O II]λ3727)/EW(Hβ) versus log EW(Hβ) and EW([O II]λ3727)/EW(Hβ) versus log EW([O II]λ3727) diagnostic diagrams. The use of equivalent widths instead of line ratios is particularly useful when the ELGs spectra are not flux calibrated. This method was tested using the Canada-France Redshift Survey $0 < z \leq 0.3$ ELGs sample. A good agreement was found between the classification obtained with this method and the results determined using the standard diagnostic diagrams (Tresse *et al.* 1996).

Although the level of discrimination obtained by the new diagnostic diagrams seems good, we have to be careful when aplying them to high redshift samples. In the case of H II galaxies it is complicated to accurately predict how galaxy evolution will affect both the $C_{3727} - C_{4861}$ colour index and the equivalent widths of the [O II]λ3727 $\AA$ and Hβ lines beyond $z = 0.3$. For AGNs it is just not possible to predict their spectral evolution with look-back time, as the mechanisms responsible for the energy generation and ionisation in these objects are still not well understood.

Undoubtedly, following work will bring a clearer view on the correlation of these observable quantities with the physical phenomena occurring in distant ELGs. Furthermore, it will be very important to be able to predict the evolution of all the observable spectral quantities with redshift, for H II galaxies, Seyferts 2 and LINERs, taking into account both stellar and nebular contributions to the observed integrated spectra. The application of these new methods to the large database of optical/near UV spectra of ELGs with $0 < z \leq 0.7 - 0.8$ currently available will allow to take a step forward in this direction and into the physical interpretation of galaxy evolution with look-back time.

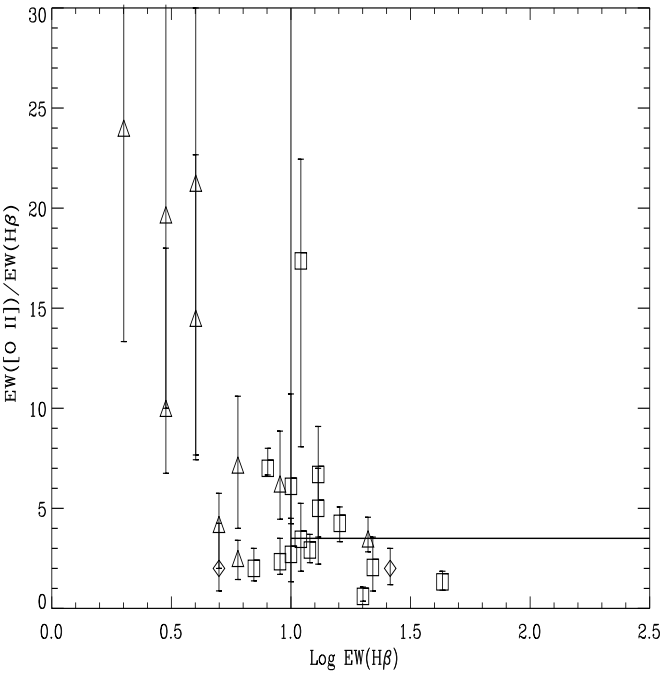

Figure 6. CFRS data plotted in our diagnostic diagram EW([O II]λ3727)/EW(Hβ) versus log EW(Hβ). The classification is that given by Tresse *et al.* (1996): squares are H II galaxies, triangles are active galaxies and diamonds are intermediate (or transition) objects.

ACKNOWLEDGMENTS

Discussions with Timothy Heckman, Richard Ellis, Robert Kennicutt, Joseph Shields, François Hammer, Guillermo Tenorio-Tagle, Luis Ho and Ilídio Lopes are gratefully acknowledged. CR thanks the support of the "Junta Nacional de Investigação Científica e Tecnológica" (Portugal) through a grant BPD/6064/95, PRAXIS XXI program. ET thanks the hospitality of the Royal Greenwich Observatory. Financial support from an ANTARES (E.C.) grant is also acknowledged.

REFERENCES

Baldwin, J., Philips, M. , & Terlevich, R., 1981, *Publs astr. Soc. Pacif.*, **93**, 5
Balick, B. & Snedon, C., 1976, *Astrophys. J.*, **208**, 336
Broadhurst, T., Ellis, R. S. & Shanks, T., 1988, *Mon. Not. R. astr. Soc.*, **235**, 827
Colless, M., Ellis, R., Taylor, K. & Hook, R. N., 1990, *Mon. Not. R. astr. Soc.*, **244**, 408
Colless, M., Ellis, R. S., Broadhurst, T., Taylor, K., Peterson, B. A. , 1993, *Mon. Not. R. astr. Soc.*, **261**, 19
Costero, R. & Osterbrock, D. E., 1977, *Astrophys. J.*, **211**, 675
Couch, W. J. & Sharples, R. M., 1987, *Mon. Not. R. astr. Soc.*, **229**, 423
Dressler, A. & Gunn, J. E., 1983, *Astrophys. J.*, **270**, 7
Filippenko, A. V., Terlevich, R. J., 1993, *Astrophys. J.*, **397**, L79
Glazebrook, K., Ellis, R., Colless, M., Broadhurst, T., Allington-Smith, J., Tanvir, N., 1995, *Mon. Not. R. astr. Soc.*, **273**, 157
Kennicutt, R. C., 1992, *Astrophys. J.*, **388**, 310
Kurucz, R., 1992, in *"The stellar population of galaxies"*, eds. Barbuy B. and Renzini A., Kluwer Academic Publishers, 225
Lavery, R. & Henry, J. P., 1988, *Astrophys. J.*, **330**, 596
Le Fèvre, O., Crampton, D., Lilly, S., Hammer, F., Tresse, L., 1995, *Astrophys. J.*, **455**, 60
Masegosa, J., Moles, M. & Campos-Aguilar, A., 1994, *Astrophys. J.*, **420**, 576
Heckman, T. M., 1980, *Astr. Astrophys.*, **87**, 152
Ho, L., Filippenko, A. V., Sargent, W. L. W., 1993, *Astrophys. J.*, **417**, 63
Rola, C. S., 1995, Ph.D. thesis, Université de Paris VII, France
Shields, G. A. & Searle, L., 1978, *Astrophys. J.*, **222**, 821
Songaila, A., Cowie, L. L., Hu, E. M., Gardner, J. P., 1994, *Astrophys. J.Suppl.*, **94**, 461
Terlevich, R., Melnick, J., Masegosa, J., Moles, M., Copetti, M., 1991, *Astr. Astrophys. Suppl.*, **91**, 285
Stasińska, G., 1990, *Astr. Astrophys. Suppl.*, **83**, 501
Terlevich, R., Melnick, J., Moles, M., 1987, *121st IAU Symp.: Ob-*

servational Evidence of Activity in Galaxies, eds. Khachikian, E., Fricke, K., Melnick, J., D. Reidel Publs. Comp., 499
Tresse, L., Rola, C. S., Hammer, F., Stasiǹska, G., Le Fèvre, O., Lilly, S., Crampton, D., 1996, *Mon. Not. R. astr. Soc.*, **281**, 847
Veilleux, S. & Osterbrock, D., 1987, *Astrophys. J. Suppl.*, **63**, 295

This paper has been produced using the Royal Astronomical Society/Blackwell Science LaTeX style file.